Journal of Information Hiding and Multimedia Signal Processing ©2016 ISSN 2073-4212
Ubiquitous International Volume **7**, Number **6**, November **2016**

NSCT-Based Multimodal Medical Image Fusion With Sparse Representation and Pulse Coupled Neural Network

Lu Tang[1,2], Leida Li[2], Jiansheng Qian[2], Jianying Zhang[2*], Jeng-Shyang Pan[3]

[1] School of Medical Imaging
Xuzhou Medical University
Xuzhou, 221004, China
tanglu@cumt.edu.cn

[2] School of Information and Electrical Engineering
China University of Mining and Technology
Xuzhou, 221116, China

[3] College of Information Science and Engineering
Fujian University of Technology
Fuzhou, 350118, China
*Corresponding author: Zjycumt@126.com

Received May, 2016; revised August, 2016

Abstract. *Multimodal medical image fusion plays a vital role in clinical diagnosis and treatment planning. In the image fusion methods based on nonsubsampled contourlet transform (NSCT) and pulse coupled neural network (PCNN), authors have used normalized coefficient value to motivate the PCNN-processing, which makes the fused image blurred, detail loss and decrease in contrast. In this paper, we present a novel multimodal medical image fusion method by combining sparse representation (SR) and pulse coupled neural network (PCNN) in nonsubsampled contourlet transform (NSCT) domain. Firstly, the source images are decomposed into low- and high-frequency bands in NSCT domain, which are sparsely represented with learned dictionaries. Then ℓ_1-norm matrix is used to motivate the PCNN-processing both in low- and high-frequency bands, and large firing times are selected as coefficients of the fused image. Finally, the fused image is reconstructed by performing inverse NSCT. Experimental results show that the proposed scheme outperforms the state-of-the-art methods in subjective quality and objective evaluation criteria.*

Keywords: Multimodal medical image fusion, Sparse representation, Pulse coupled neural network, Nonsubsampled contourlet transform.

1. **Introduction.** To provide more accurate comprehensive pathological information to doctors for better diagnosis and treatment, multimodal medical image fusion has become an important issue in medical image analysis. There are various modalities such as X-ray Computed Tomography (CT), Magnetic Resonance Imaging (MRI) T1, T2 sequences, Ultrasonography, Positron Emission Tomography (PET) and Single Photon Emission Computed Tomography (SPECT). Different imaging modalities reflect different aspects of human body information. For example, CT images can show dense structures like bones and implants with less distortion, but cannot detect physiological changes, while MR images can provide normal and pathological soft tissues information, but cannot provide the

bones information [1]. Multimodal medical image fusion offers an important approach to solve this problem by integrating complimentary features of different imaging modalities into one fused image. In the past few years, various multimodal medical image fusion algorithms have been addressed in the literature. These approaches can be classified into spatial and transform domain [2]. Spatial domain algorithms include average, variance, energy of image gradient, sum modified Laplacian and spatial frequency [3]. The transform domain fusion methods use a decomposition-fusion-reconstruction framework [4]. Classical transform domain fusion methods include principal component analysis (PCA) [5], gradient pyramid (GP) [6], discrete wavelet transform (DWT), dual-tree complex wavelet transform (DTCWT) [7-8], and multi-scale geometric analysis like curvelet transform (CVT) [9] and nonsubsampled contourlet transform (NSCT) [10]. Among these transforms, NSCT is shift-invariant and can suppress pseudo-Gibbs phenomena during fusion, so it is more suitable for image fusion. However, how to measure the importance/contribution of individual source image in the fused image, and to find a more effective way of combination is still an open problem [11]. Recently, attempts have been made to integrate NSCT with other techniques for more effective medical image fusion [1, 12]. Pulse coupled neural network (PCNN), which is a biologically inspired spiking neural network based on cats visual cortex has been utilized in image fusion [13-14]. The basic PCNN model is utilized in NSCT domain [15]. Modified spatial frequency-motivated PCNN has been adapted in NSCT domain [16]. Among these methods, external stimulus to PCNN for approximate and detail sub-bands is normalized coefficient value. In fact, the information present in approximate and detail sub-bands are different, the normalized coefficient value used to motivate PCNN leads to blur and loss of details in the fused image, moreover the parameters of PCNN are fixed, which are not applicable to different medical image modalities. Medical images of different modalities contain large amount of edges and directional features, which are quite often very subtle in nature. NSCT is a shift invariant MSD transform that has high directional sensitivity, which is able to represent the smoothness along the edges or contours properly. These features of NSCT are suitable for medical image fusion application. The parameters of PCNN play important roles in the model. Once the input images are changed, the defined parameters may no longer be suitable for the new images. To make full use of the biological characteristics of PCNN, we combine the PCNN properties and the image characteristics to adaptively determine the linking strength. This inspired us to propose a new image fusion methodology in NSCT domain that is superior to the current methods which do not capture edges spectral information and detail features in a satisfactory manner for multimodality medical images.

Electrophysiological experiments on the primate temporal visual cortex and catvisual cortex [17-19] have shown that the neuronal representation of complex stimulus in visual cortex is based on sparse coding. Sparse representation (SR) addresses signals natural sparsity, which is consistent with the physiological characteristics of the human visual system. SR can extract more effective features for image analysis. In this paper, an efficient multimodal medical image fusion algorithm combining SR and PCNN in NSCT domain is proposed. Firstly, the source images are decomposed into low frequency bands (LFS) and high frequency bands (HFS) in NSCT domain, which are then sparsely represented with learned dictionary. Then ℓ_1 -norm matrix is used to motivate the PCNN-processing both in low- and high- frequency bands with adaptive linking strength, and large firing times are selected as fusion rule. Finally, inverse NSCT is conducted to obtain the fused image.

2. **Related Works.**

2.1. **NonSubsampled Contourlet Transform.** NSCT is a shift-invariant, multiscale, and multidirection image decomposition transform. It is based on the non-subsampled pyramid filter bank (NSP or NSPFB) and the non-subsampled DFB (NSDFB) [20]. The NSP performs multiscale decomposition, which divides an image into a low frequency sub-band and a high frequency sub-band at each NSP decomposition by using two-channel non-subsampled filter bank, as a result, NSP generates k+1 sub-images, which consist of one low frequency image and k high frequency images having the same size as source image, where k denotes the number of decomposition levels. NSDFB provides direction decomposition, which decomposes the high frequency sub-bands from NSP in each level and 2^l directional sub-images with the same size as the source image are obtained, where l is the number of decomposition directions. Therefore, NSDFB offers the NSCT with more precise directional detail information.

2.2. **Sparse Representation.** The basic principle of sparse representation is that a signal can be expressed as a sparse linear combination of a few atoms from an overcomplete dictionary. In the sparse linear model, one patch of an image can be represented as a column vector $\mathbf{v}$ in the dictionary $\mathbf{D}$. That is $\mathbf{v}$=$\mathbf{Dx}$, where $\mathbf{x} \in \mathbf{R}^m$ is the sparse coefficients of $\mathbf{v}$. Let $\mathbf{D}$=($\mathbf{d}_1$,$\mathbf{d}_2$,...,$\mathbf{d}_m$) $\in \mathbf{R}^{n\times m}$, each column of $\mathbf{D}$ is an atom, we say that the dictionary $\mathbf{D}$ is redundant when the number of atom m is much larger than the dimension of an atom n. The dictionary $\mathbf{D}$ can be obtained using dictionary learning methods, such as K-SVD [21] and MOD [22]. The target of SR is to calculate the representation vector $\mathbf{x}$ which contains the fewest nonzero entries. Let denote the number of the nonzero entries in $\mathbf{x}$, the above discussion can be formulated as follows:

$$\min_{\mathbf{x}} \| \mathbf{x} \|_0, \quad s.t. \quad \| \mathbf{v} - \mathbf{Dx} \|_2^2 < \varepsilon \tag{1}$$

where $\varepsilon > 0$ is the error tolerance parameter. Solving the sparse representation problems (1) is generally NP-hard. Some effective pursuit methods, such as Orthogonal Matching Pursuit (OMP) [23] and Basis Pursuit (BP) [24] have been proposed to solve this problem. In this paper, we employ BP to do the sparse representation. BP is a convex relaxation algorithm defined as

$$\min_{\mathbf{x}} \| \mathbf{x} \|_1, \quad s.t. \quad \| \mathbf{v} - \mathbf{Dx} \|_2^2 < \varepsilon \tag{2}$$

where $\| \cdot \|_1$ denotes ℓ_1 -norm of vectors, which is the sum of absolute values of all elements.

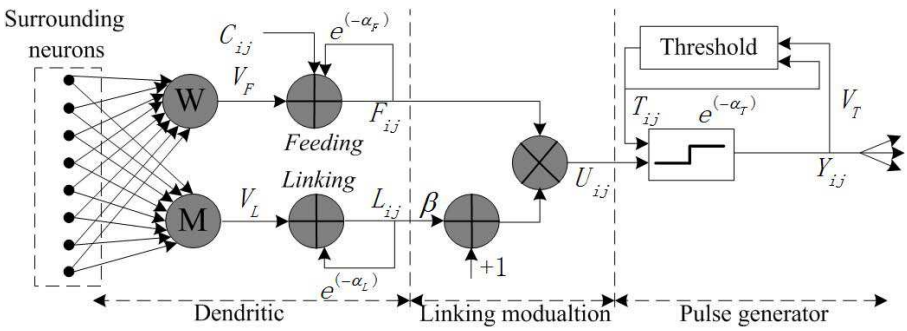

FIGURE 1. Structure of the PCNN neuron model

2.3. **Pulse Coupled Neural Network.** PCNN is a biologically inspired neural network, which is similar with the mode of human visual processing, so PCNN fusion rule is exploited to fuse the sparse coefficients of source images. The structure of a PCNN neuron model is shown in Fig. 1. It consists of three modules [14]: the dendritic tree, the linking modulation and the pulse generator, the dendritic module comprises of two input parts: feeding input and linking input, the feeding receives external stimulus and local stimulus, while the linking receives external stimulus from the output of surrounding neurons, as represented as Eq.(3) and (4):

$$F_{i,j}(n) = e^{-\alpha_F} F_{i,j}(n-1) + V_F \sum_{k,l} W_{i,j,k,l} Y_{i,j}(n-1) + C_{i,j} \tag{3}$$

$$L_{i,j}(n) = e^{-\alpha_L} L_{i,j}(n-1) + V_L \sum_{k,l} M_{i,j,k,l} Y_{i,j}(n-1) \tag{4}$$

where W and M are the synaptic weight matrices and $C_{i,j}(n)$ is the external stimulus. V_F and V_L are normalizing constants, α_F and α_L are the time constants (α_F<α_F). The linking modulation is given by:

$$U_{i,j}(n) = F_{i,j}(n)[1 + \beta L_{i,j}(n)] \tag{5}$$

In Eq.(5), $U_{i,j}(n)$ is total internal activity of the neuron. β is the linking parameter and the pulse generator determines the firing events in the model in Eq.(6). $Y_{i,j}(n)$ depends on the internal state and threshold.

$$Y_{i,j}(n) = \begin{cases} 1, & U_{i,j}(n) > T_{i,j}(n) \\ 0, & U_{i,j}(n) \leq T_{i,j}(n) \end{cases} \tag{6}$$

The dynamic threshold of the neuron is formulated as Eq.(7).

$$T_{i,j}(n) = e^{-\alpha_T} T_{i,j}(n-1) + V_T Y_{i,j}(n) \tag{7}$$

where V_T is normalized constant and α_T is time constant.

3. **Proposed Fusion Rule.** An efficient NSCT-domain image fusion algorithm combining SR and PCNN named NSCT-SR-PCNN, is presented. The source images are firstly decomposed into low and high frequency bands by NSCT. Each subband is subsequently sparsely represented with learned dictionary, and ℓ_1-norm matrix is used to motivate the PCNN-processing both in low and high frequency bands, large firing times are selected as coefficients of the fused image. Finally, the fused image is obtained by performing the INSCT over the merged coefficients. The schematic diagram of the proposed image fusion framework is depicted in Fig. 2.

3.1. **Definition of ℓ_1-norm Matrix.** The source images are firstly decomposed into low and high frequency bands by NSCT, applying the sliding window technique to divide every sub-band into image patches of size n × n from upper left to lower right with a step length of s pixels. For each position p of patches, the pixel values of every patch are lexicographic ordered into a column vector $\{\mathbf{V}^p\}$, Calculating the sparse coefficient vectors $\{\mathbf{Q}^p\}$ of $\{\mathbf{V}^p\}$ using BP algorithm by

$$\mathbf{Q}^p = \min_{\mathbf{x}} \| \mathbf{Q} \|_1, \quad s.t. \quad \| \mathbf{V}^p - \mathbf{D}\mathbf{x} \|_2^2 < \varepsilon \tag{8}$$

the dictionaries $\mathbf{D}$ both are used for (LFS) and (HFS). $\| \cdot \|_1$ denotes ℓ_1-norm, which is the sum of absolute values of all elements. Supposing source image size $l \times w$, center coordinate of patch $p(x_p , y_p)$, which is defined as:

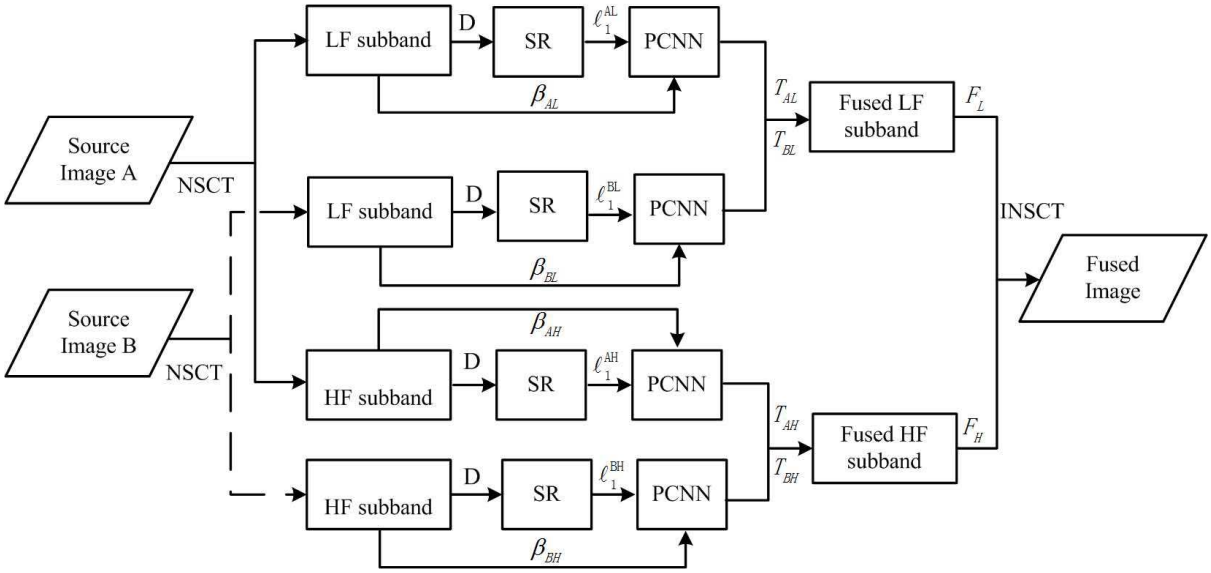

FIGURE 2. Schematic diagram of the proposed image fusion framework

$$\begin{cases} x_p = [(p-1) mod(\lfloor w/s \rfloor)] \times s + \lceil n/2 \rceil \\ y_p = [\lfloor (p-1)/(\lfloor w/s \rfloor) \rfloor] \times s + \lceil n/2 \rceil \end{cases} \tag{9}$$

From ℓ_1-norm, we can compute ℓ_1-norm matrix, which is defined as:

$$\ell_1(i,j) = \begin{cases} \| \mathbf{Q}^p \|_1 & if \quad i = x_p \ \ and \ \ j = y_p \\ 0 & otherwise \end{cases} \tag{10}$$

3.2. **Definition of Directional Gradient Feature.** The linking parameter β is an important parameter which varies the weightage of linking field. Sum of directional gradients feature (SDG) at each location in contourlet domain is considered as the linking strength of the neuron present in the corresponding location. The sum of directional gradients of a function I(x, y) is defined as:

$$\begin{aligned} \beta = SDG[I(x,y)] = &\sqrt{[I(x,y) - I(x-1,y)]^2 + [I(x,y) - I(x+1,y)]^2} \\ &+ \sqrt{[I(x,y) - I(x,y-1)]^2 + [I(x,y) - I(x,y+1)]^2} \\ &+ \sqrt{[I(x,y) - I(x-1,y-1)]^2 + [I(x,y) - I(x+1,y+1)]/2} \\ &+ \sqrt{[I(x,y) - I(x-1,y+1)]^2 + [I(x,y) - I(x+1,y-1)]/2} \end{aligned} \tag{11}$$

3.3. **NSCT-SR-PCNN.** The detailed fusion scheme is summarized as follows: The two source images A and B are represented in low-frequency sub-bands (LFS) $\{AL, BL\}$ and high-frequency (HF) sub-bands $\{AH, BH\}$ by using NSCT. Applying the sliding window technique to divide AL, BL, AH, BH into image patches, For each position p of patches, the pixel values of every patch are lexicographic ordered into a column vector $\{\mathbf{V}^p_{AL}$, $\mathbf{V}^p_{BL}$, $\mathbf{V}^p_{AH}$, $\mathbf{V}^p_{BH}\}$. Calculate the sparse coefficient vectors $\{\mathbf{Q}^p_{AL}$, $\mathbf{Q}^p_{BL}$, $\mathbf{Q}^p_{AH}$, $\mathbf{Q}^p_{BH}\}$ of $\{\mathbf{V}^p_{AL}$, $\mathbf{V}^p_{BL}$, $\mathbf{V}^p_{AH}$, $\mathbf{V}^p_{BH}\}$using Eq.(8), get $\{\ell_1^{AL}$, ℓ_1^{BL}, ℓ_1^{AH}, $\ell_1^{BH}\}$ using Eq.(9)-(10). Input ℓ_1-norm matrix of each LFS and HFS to motivate the PCNN-processing, that is ℓ_1 (i,j) $=C_{i,j}$, and generate pulse of neurons with Eq.(3)-(6), Calculate $\{\beta_{AL}$, β_{BL}, β_{AH}, β_{BL} $\}$using Eq.(11), on the basis of the firing time that is evaluated in Eq.(7), we can compute

the time matrices of PCNN-processing LF sub-bands AL, BL as T_{AL}, T_{BL}, respectively. Similarly, we can get T_{AH} and T_{BH}. Fuse the coefficients of the LFS by the following fusion rule:

$$F_L = \begin{cases} \max(AL, BL) & T_{AL} = T_{BL} \\ AL & T_{AL} > T_{BL} \\ BL & T_{AL} < T_{BL} \end{cases} \tag{12}$$

from Eq.(12), we can get F_H, where F_L and F_H are the fused image of LFS and HFS, respectively. Perform the inverse NSCT over F_L and F_H to reconstruct the final fused image F.

4. **Experiments Result Analysis.** To evaluate the performance of the proposed approach, the experiments on four pairs of multimodal medical images are conducted in Fig. 3, which can be downloaded from http://www.imagefusion.org and http://www.med.harvard.edu/aanlib/home.html. All images have the same size of 256 × 256 pixels, with 256-level gray scale. These pair images are divided into four groups. (A): MRI-T1 and Gd-DTPA-MRI-T2, (B): B ultrasound and SPECT, (C): CT and MRI, (D): MRI-T1 and MRI-T2. In the experiments, the proposed method is compared with following five fusion algorithms, including image fusion with guided filtering (GFF) [25], a general framework for image fusion based on multi-scale transform and sparse representation (LP-SR) [26], nsct-based multimodal medical image fusion using pulse-coupled neural network and modified spatial frequency (NSCT-PCNN-SF) [16], image fusion algorithm based on spatial frequency-motivated pulse coupled neural networks in nonsubsampled contourlet transform domain (NSCT-SF-PCNN) [15], medical image fusion by combining nonsubsampled contourlet transform and sparse representation (NSCT-SR) [27]. For fair comparison, we use the parameters that were reported by the authors to yield the best fusion results.

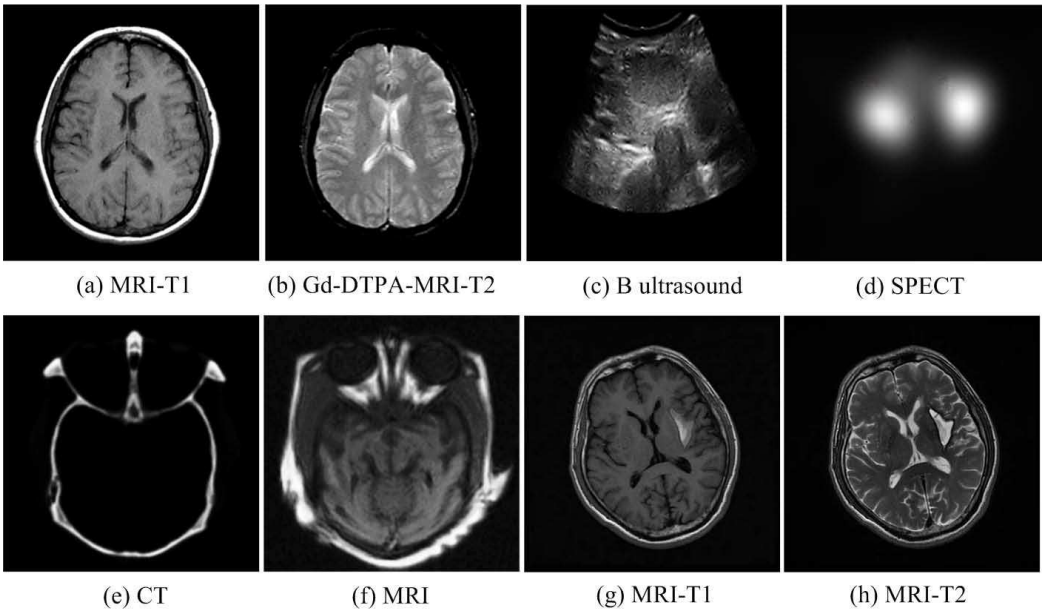

FIGURE 3. Source multimodal medical images for fusion experiments

Figs. 4-7 show the fused images by the proposed method and the other five methods. From the fusion results in Fig. 4(a)-4(f), it is clear that the image fused by our method reaches a higher contrast among all the fused images, which cannot be seen in the original

MRI-T1 or Gd-DTPA-MRI-T2 image. Fig. 4 show two source medical images captured using T1-weighted MR and T2-weighted MR-GAD image of several focal lesions involving basal ganglia (Gd-DTPA-MRI-T2) respectively. From Fig. 4(a), (c) and (d), it can be seen that in the results produced by the GFF, NSCT-PCNN-SF and NSCT-SF-PCNN method, some edge detail structures are invisible, some details blur in Fig. 4(b) and (e), the results of above five method may decrease the brightness of soft-tissue structures, thus make some details blur and several focal lesions are not clear (highlighted by white arrows). From the fusion results in Fig. 4(a)-4(f), it is clear that the image fused by our proposed algorithm not only preserves edge spectral information but also improves the spatial detail information (highlighted by red arrows). At the same time, the pathology of brain which is lacunar infarction in this case is presented clearly over all existing algorithms.

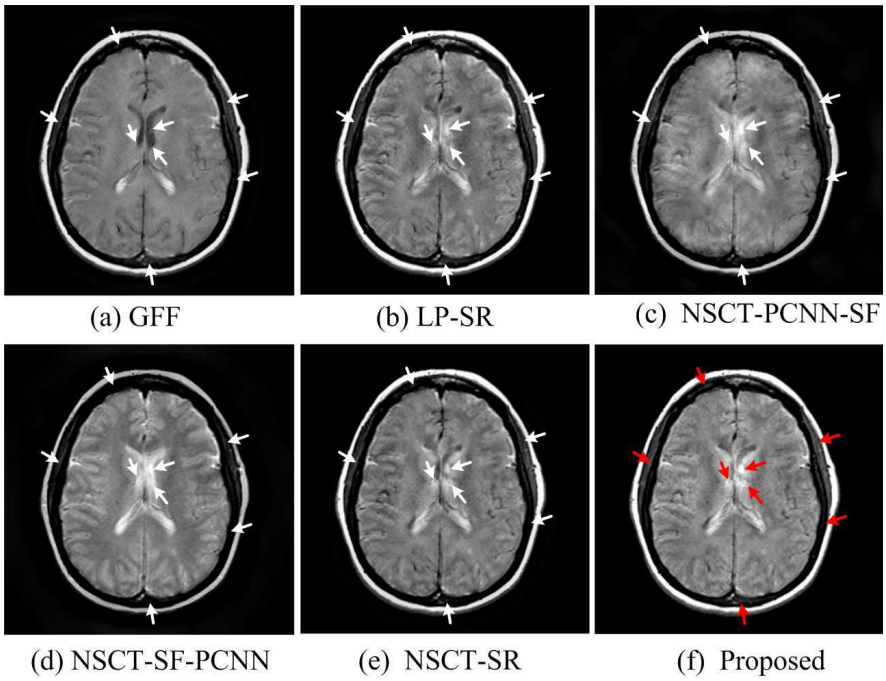

FIGURE 4. Fusion results of groups (A)

The fusion results of the six algorithms in Fig. 5(a)-5(f) show that our method has the best visual effect in all the fusion methods, which cannot be seen in the separate B ultrasound or SPECT image. Fig. 5(a)-5(d) show that GFF, LP-SR, NSCT-PCNN-SF, and NSCT-SF-PCNN cannot fuse this type of medical images well; Figure 5(e) shows that NSCT-SR method can get much better performances. Compared with the fused images of NSCT-SR, the proposed fusion algorithm preserves the texture information of source images well. Similar performance is perceived for the remaining two groups (group (C) and group (D)), which are shown in Fig. 6 and Fig. 7, respectively.

The comparisons show that the proposed scheme is most effective among the six algorithms. For further comparison except for the visual observation above, popular objective metrics are utilized to evaluate the quality of fused image quantitatively, including mutual information(MI) [1,15], standard deviation(SD) [25], spatial frequency(SF) [1,15], gradient(Q_G) [25]. These four performance indexes can effect evaluate the quality of fused image quantitatively. MI indicates the amount of information contained in the fused image about the source images. SD is mainly used to measure the overall contrast of the fused image. SF indicates the overall activity of fused image. Q_G evaluate the

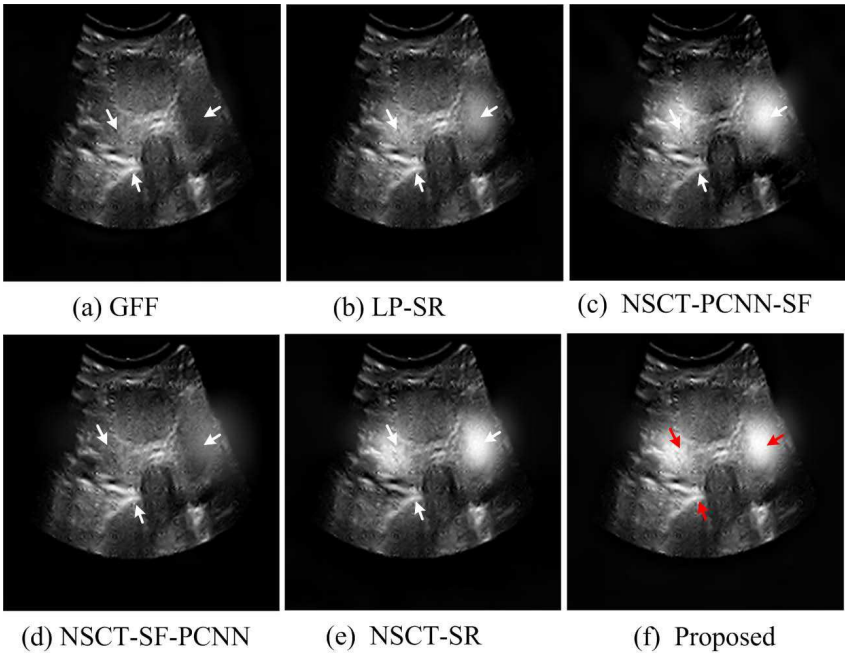

FIGURE 5. Fusion results of groups (B)

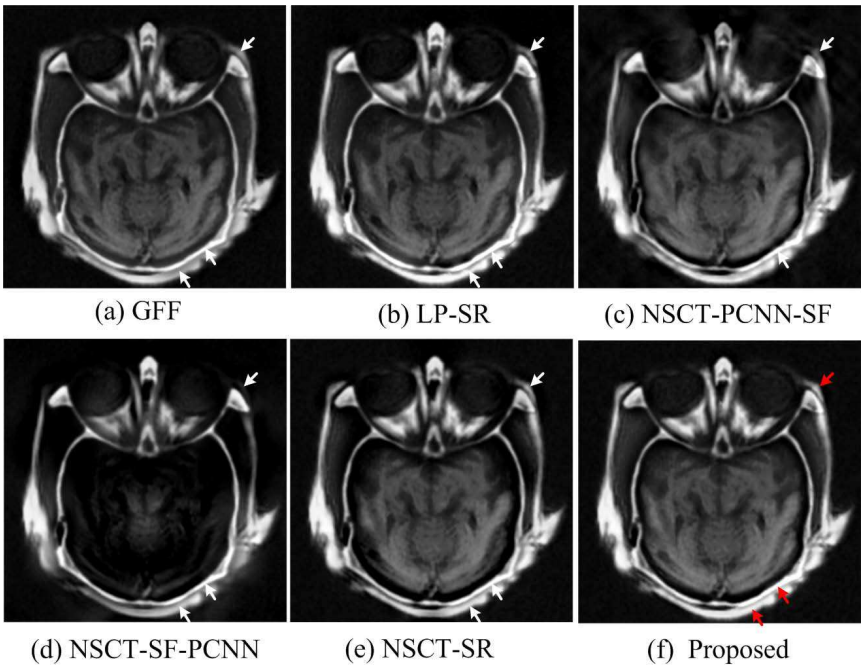

FIGURE 6. Fusion results of groups (C)

success of edge information or gradient information injected into the fused image from the source images. In general, the larger the values of MI, SD, SF and Q_G indicate better fusion quality. Table 1 summarizes the simulation results of the proposed method and five state-of-the-art methods, where the best result is marked in boldface. It is known from Table 1 that the proposed method produces the best results in Group (A) and Group (B). In Group (C), MI and SF values of the proposed algorithm are best. In Group D, this observation clearly suggests that Q_G values is only slightly worse than LP-SR, the MI, SD, SF values of proposed method are superior to all the other methods. From these

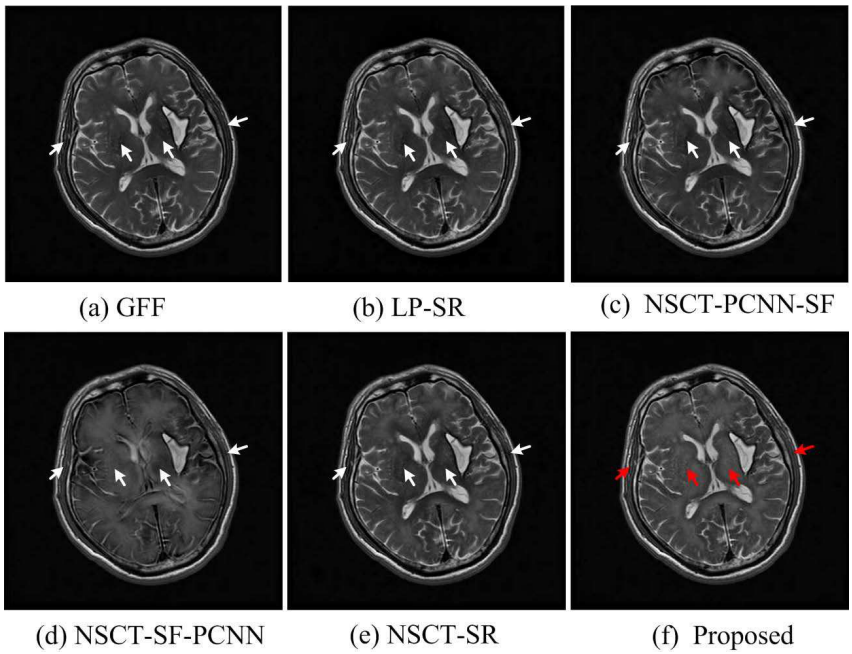

FIGURE 7. Fusion results of groups (D)

experiments, we may draw the conclusion that the proposed method is better than the other methods, which should attribute to the saliency medical images which is captured by sparse representation and ℓ_1-norm matrix to activate the PCNN.

TABLE 1. Objective criteria on the multimodal medical images fusion results

Source Images	metric	GFF	LP-SR	NSCT-PCNN-SF	NSCT-SF-PCNN	NSCT-SR	proposed
Group (A) MRI-T1, Gd-DTPA-MRI.T2	**MI**	2.8330	2.8899	2.5052	2.9447	2.7265	**2.9517**
	SD	64.9513	67.8278	66.4747	65.4124	66.5807	**72.5448**
	SF	5.9151	6.6913	6.1888	6.1476	6.4312	**6.8566**
	$\mathbf{Q}_G$	0.6378	0.7193	0.4752	0.5028	0.6557	**0.7222**
Group (B) B ultrasound, SPECT	**MI**	3.4735	3.5531	2.8597	3.2090	3.7118	**4.3099**
	SD	39.7509	44.7922	49.6209	42.0263	50.2828	**52.9381**
	SF	6.5647	6.6016	6.5376	6.5959	6.6851	**6.6882**
	$\mathbf{Q}_G$	0.7300	0.7366	0.5285	0.7225	0.7402	**0.7525**
Group (C) CT, MRI	**MI**	3.4307	3.1260	2.2030	1.2819	3.0118	**3.5891**
	SD	53.5610	**59.9399**	55.6074	51.8312	56.3958	58.9436
	SF	6.5492	6.7673	6.5828	6.0079	6.7428	**6.8128**
	$\mathbf{Q}_G$	**0.8070**	0.7898	0.4970	0.4245	0.7302	0.8066
Group (D) MRI-T1, MRI-T2	**MI**	4.3961	3.8387	3.9109	4.1132	4.3043	**4.4155**
	SD	38.7853	40.4644	39.0230	35.5550	40.4137	**42.4488**
	SF	5.3905	5.5128	5.4383	5.0013	5.4957	**5.6798**
	$\mathbf{Q}_G$	**0.7694**	0.7195	0.6403	0.6840	0.7335	0.7645

5. **Conclusion.** In this paper, a new multimodal medical image fusion algorithm which combines SR and PCNN in NSCT domain has been presented. To integrate as much information as possible into the fused images, we exploit the multi-scale and multi-directional properties of NSCT and SR along with ℓ_1-norm matrix motivated PCNN to capture the subtle differences as well as the fine details present in the source multimodal medical images into the fused image. The experiments have shown that the proposed scheme outperforms the state-of-the-art fusion methods in terms of both the subjective and objective performance valuation.

Acknowledgment. The authors would like to thank both the editor and the reviewers for the invaluable comments and suggestions. This work has been supported by the Xu Zhou Science and technology Program under the Grant No.KC14SH078 and KC15SH019, and the Qing Lan Project.

REFERENCES

[1] P. Ganasala · V. Kumar, CT and MR Image Fusion Scheme in Nonsubsampled Contourlet Transform Domain, *Journal of Digital Imaging*, vol. 27, pp. 407-418, 2014.
[2] T. Stathaki, Image Fusion: Algorithms and Applications, *Academic Press*, 2011.
[3] N. V. Gangapure, S. Banerjee, A. S. Chowdhury, Steerable Local Frequency Based Multispectral Multifocus Image Fusion, *Information Fusion*, no. 23, pp. 99-115, 2015.
[4] G. Piella, A General Framework for Multiresolution Image Fusion: From Pixels to Regions, *Information Fusion*, vol. 4, no. 4, pp. 259-280, 2003.
[5] C. Duan, Q. H. Huang, X. G. Wang, S. Wang, Remote Image Fusion Based on PCA and Dual Tree Compactly Supported Shearlet Transform, *Journal of Information Hiding and Multimedia Signal Processing*, vol. 5, no. 3, pp. 485-496, 2014.
[6] V. Petrovic, C. Xydeas, Gradient-based Multiresolution Image Fusion, *IEEE Transactions on Image Processing*, vol. 13, no. 2, pp. 228-237, 2004.
[7] Y. Yang, S. Huang, J. Gao, Z. Qian, Multi-focus Image Fusion Using An Effective Discrete Wavelet Transform Based Algorithm, *Measurement Science Review*, vol. 14, no. 2, pp. 102-108, 2014.
[8] J. Lewis, R. OCallaghan, S. Nikolov, D. Bull, N. Canagarajah, Pixel and Region Based Image Fusion with Complex Wavelets, *Inform Fusion*, vol. 8, no. 2, pp. 119-130, 2007.
[9] F. Nencini, A. Garzelli, S. Baronti, Remote Sensing Image Fusion Using the Curvelet Transform, *Inform Fusion*, no. 8, pp. 143-156, 2007.
[10] A. L. Cunha, J. P. Zhou, M. N. Do, The Non-subsampled Contourlet Transform: Theory, Design and Applications, *IEEE Transactions on Image Process*, no. 15, pp. 3089-3101, 2006.
[11] S. Das, M. K. Kundu, A Neuro-Fuzzy Approach for Medical Image Fusion, *IEEE Transactions on Biomedical Engineering*, vol. 60, no. 12, pp. 3347-3353, 2013.
[12] G. Yang, M. Li, L. Chen, J. Yu, The Nonsubsampled Contourlet Transform Based Statistical Medical Image Fusion Using Generalized Gaussian Density, *Computational and Mathematical Methods in Medicine*, pp. 1-13, 2015.
[13] Z. Wang, Y. Ma, F. Cheng, L. Yang, Review of Pulse-coupled Neural Networks, *Image and Vision Computing*, vol. 28, no. 1, pp. 5-13, 2010.
[14] Z. Wang, Y. Ma, Medical Image Fusion Using m-PCNN, *Information Fusion*, vol. 9, pp. 176-185, 2008.
[15] X. Qu, J. Yan, H. Xiao, Image Fusion Algorithm Based on Spatial Frequency-Motivated Pulse Coupled Neural Networks in Nonsubsampled Contourlet Transform Domain, *Acta Automatica Sinica*, vol. 34, no. 12, pp. 1508-1514, 2008.
[16] S. Das · M. K. Kundu, NSCT-based Multimodal Medical Image Fusion Using Pulse-coupled Neural Network and Modified Spatial Frequency, *Medical and Biological Engineering and Computing*, vol. 50, pp. 1105-1114, 2012.
[17] E. T. Rolls, M. J. Tovee, Sparseness of The Neuronal Representation of Stmuli in The Primate Temporal Visual Cortex, *Journal of Neurophysiology*, vol. 73 no. 2, pp. 713-726, 1995.
[18] D. Ferster, S. Chung, H. Wheat, Orientation Selectivity of Thalamic Input to Simple Cells of Cat Visual Cortex, *Nature*, vol. 380, pp. 249-252, 1996.
[19] B. A. Olshausen, D. J. Field, Emergency of Simple-cell Receptive Field Proper Ties by Learning A Sparse Code for Natural Images, *Nature*, vol. 381, pp. 607-609, 1994.
[20] P. Geng, S. Tian, K. Lu, Multifocus Image Fusion by Sum of Local Variance Energy, *Journal of Information Hiding and Multimedia Signal Processing*, vol. 7, no. 1, pp. 175-183, 2016.
[21] M. Aharon, M. Elad, A. Bruckstein, K-svd: An Algorithm for Designing Overcomplete Dictionaries for Sparse Representation, *IEEE Transactions on Signal Process*, vol. 54, no. 11, pp. 4311-4322, 2006.
[22] K. Engan, S. O. Aase, J. H. Husoy, Multi-frame Compression: Theory and Design, *Signal Process*, vol. 80, no. 10, pp. 2121-2140, 2000.
[23] S. Mallat, Z. Zhang, Matching Pursuits with Time-frequency Dictionaries, *IEEE Transactions on Signal Process*, vol. 41, no. 12, pp. 3397-3415, 2006.

[24] J. A. Tropp, Greed is good: Algorithmic Results for Sparse Approximation, *IEEE Transactions on Information Theory*, vol. 50, no. 10, pp. 2231-2242, 2004.
[25] S. Li, X. Kang, J. Hu, Image Fusion with Guided Filtering, *IEEE Transactions on Image Processing*, vol. 22, no. 7, pp. 2864-2875, 2013.
[26] Y. Liu, S. Liu , Z. Wang, A General Framework for Image Fusion Based on Multi-scale Transform and Sparse Representation, *Information Fusion*, vol. 24, pp. 147-164, 2015.
[27] Y. Liu, S. Liu, Z. Wang, Medical Image Fusion by Combining Nonsubsampled Contourlet Transform and Sparse Representation, *Pattern Recognition*, vol. 484, pp. 372-381, 2014.